Water Research X 26 (2025) 100286

Contents lists available at ScienceDirect

Water Research X

journal homepage: www.sciencedirect.com/journal/water-research-x

An inconvenient impact: Unveiling the overlooked differences in crystalline forms of iron (hydro)oxides on anaerobic digestion

Han-Quan Wen [a,1], Guan-Lin Chen [a,1], Yu-Sheng Li [a,b], Tian Tian [c,*], Yuan Pan [a], Han-Qing Yu [a,*]

[a] CAS Key Laboratory of Urban Pollutant Conversion, Department of Environmental Science and Technology, University of Science and Technology of China, Hefei 230026, China
[b] Institute of Advanced Technology, University of Science and Technology of China, Hefei 230000, China
[c] Key Laboratory of Industrial Ecology and Environmental Engineering (Ministry of Education China), School of Environmental Science and Technology, Dalian University of Technology, Dalian 116024, China

ARTICLE INFO

Keywords:
Anaerobic digestion
FeOOH
crystalline form
EPS
Metagenome

ABSTRACT

Iron (hydro)oxides are commonly used to enhance anaerobic digestion due to their cost-effectiveness and versatility. However, the influence of crystalline structure on digestion performance is often overlooked despite their unique characteristics. In this study, we investigated how different crystalline forms of FeOOH affect substrate utilization, sludge activity, and the microbiomes in up-flow anaerobic sludge blanket (UASB) reactors. The crystalline structure of FeOOH impacted reactor performance, with γ-FeOOH, β-FeOOH, and α-FeOOH showing decreasing effectiveness, as reflected in chemical oxygen demand (COD) removal efficiencies of 99.0 %, 98.3 % and 97.1 %, respectively. FeOOH crystals influenced the secretion of extracellular polymeric substances (EPS) and sludge activity by releasing Fe ions at varying rates, leading to Fe accumulation in EPS in the order of β-FeOOH > γ-FeOOH > α-FeOOH. Additionally, γ-FeOOH supported the most stable microbial community structure, as indicated by the highest Alpha diversity index. This stability was associated with increased levels of *Mesotoga* and *Syntrophus*, along with the highest coenzyme F_{420} activity, which was approximately twice as high as in other groups. These findings underscore the crucial role of the crystalline structure of iron oxides in enhancing anaerobic digestion, emphasizing that biocompatibility should be a priority when optimizing digestion performance.

1. Introduction

Anaerobic digestion is widely recognized as a promising approach for reducing carbon emissions and achieving carbon neutrality (Wang et al., 2024). However, its capacity to treat complex organic wastewaters often requires enhancement. Iron oxides and hydro-oxides have emerged as a strategy for this purpose due to their cost-effectiveness and adaptable surface properties (Alatalo et al., 2019). They improve digestion performance through several mechanisms, including lowering the oxidation-reduction potential (ORP), generating hydrogen (H_2), facilitating direct interspecies electron transfer (DIET) (Zhang et al., 2023), and modifying the microbial community to enrich Fe-related microbes (Tian & Yu, 2020).

Despite their utility, the use of iron (hydro)oxides in anaerobic digestion is often generalized, overlooking the distinct properties provided by their diverse crystalline structures. Iron (hydro)oxides with highly crystalline forms, such as hematite and magnetite, have been found to enhance DIET more effectively than their less crystalline counterparts, like ferrihydrite (Brown et al., 1999; Zhou et al., 2023). This is further evidenced by magnetite's superior performance over ferric oxyhydroxide in treating cheese-processing wastewater (Brown et al., 1999) and by crystalline Fe_2O_3 outperforming amorphous Fe $(OH)_3$ in enhancing electron-transfer capacity (Wang et al., 2019). Conversely, some studies have shown that less crystalline iron (hydro) oxides can be more effective in anaerobic digestion than highly crystalline ones (Dong et al., 2017; Zhao et al., 2017). Poorly ordered crystalline iron (hydro)oxides achieved greater dissimilatory iron reduction and supported the formation of more efficient microbial consortium (Dong et al., 2017). For instance, less crystalline ferrihydrite was previously found to facilitate the activity of *Shewanella putrefaciens*

* Corresponding authors.
E-mail addresses: skyetian@dlut.edu.cn (T. Tian), hqyu@ustc.edu.cn (H.-Q. Yu).
[1] These authors contributed equally to this work.

https://doi.org/10.1016/j.wroa.2024.100286
Received 7 October 2024; Received in revised form 12 November 2024; Accepted 22 November 2024
Available online 23 November 2024

(Taillefert et al., 2007) and the enrichment of Fe(III)-reducing bacteria (Zhao et al., 2017). Therefore, iron (hydro)oxides with varying crystalline structures demonstrate complex and sometimes contradictory effects on anaerobic digestion (Bird et al., 2011).

The diverse roles of iron (hydro)oxides in anaerobic digestion are closely linked to their crystalline structures, which determine their surface properties, conductivity, and reactivity (Kato et al., 2012; Kleber et al., 2021). FeOOH, recognized for its distinct Fe(III) elemental composition and varied crystal forms (α, β, γ, and δ), serves as an ideal candidate to elucidate the differential impact of crystalline structures in anaerobic digestion (Ali et al., 2016). Moreover, FeOOH commonly appears as crystalline forms on the surface of various iron oxides, which can be directly interact with anaerobic sludge, influencing its morphology and activity, and ultimately affecting digestion performance (Furcas et al., 2023; Zhang et al., 2020). Previous studies have shown that FeOOH can enhance mass transformation in anaerobic digestion systems and promote the development of microbial communities beneficial for methanogenesis. However, these studies did not distinguish the variations among different crystalline forms (Cheng et al., 2020; Liu et al., 2023b; Qian et al., 2023; Weng et al., 2023). The crystalline form of FeOOH may impact anaerobic digestion in several ways: varying dissolution rates provide different levels of Fe ion accessibility (Liu et al., 2023a; Poulton and Canfield, 2005); the surface characteristics can influence conductivity for DIET (Otte et al., 2012); and distinct crystalline forms may alter the microbial community structures due to differences in biocompatibility and toxicity (Ma et al., 2013). Therefore, the specific roles of crystalline FeOOH in anaerobic digestion remain unclear and warrant in-depth investigation.

This study aims to highlight the overlooked differences among crystalline iron (hydro)oxides in anaerobic digestion. The roles of α, β,

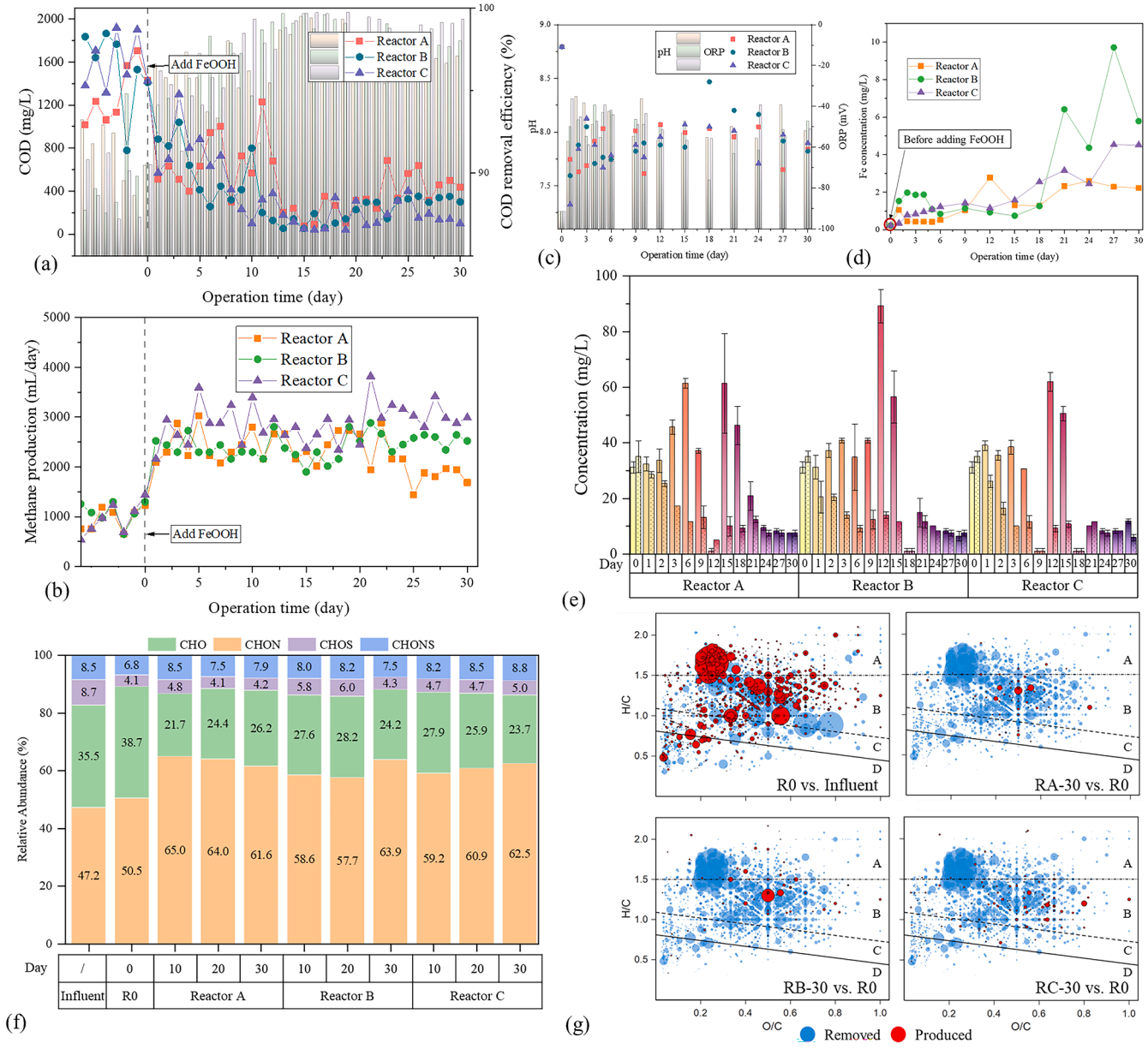

Fig. 1. Reactor operation with FeOOH addition. (a) Effluent COD and degradation efficiency. (b) Methane production. (c) pH and ORP measurements. (d) Fe concentration in the effluent. (e) VFA and ethanol concentration. (f) Relative abundance of DOM elemental composition. (g) Removed and produced DOM molecules among different samples (R0 vs. influent, RA on Day 30 vs. R0, RB on Day 30 vs. R0, RC on Day 30 vs. R0), categorized into aliphatic compounds (A), highly unsaturated compounds (B), polyphenols (C), and polycyclic aromatics (D). The size of each circle represents the relative intensities of molecules, with blue indicating degradation and red indicating production.

and γ-FeOOH were specifically investigated in UASB reactors treating reconstituted tobacco leaf production waste, with a comparative analysis of their effects on extracellular polymeric substances (EPS), sludge activity, and the microbiome. Through this comprehensive approach, we intend to deepen the understanding of how variations in crystalline iron (hydro)oxides impact anerobic digestion and address a critical gap in current research.

2. Results

2.1. UASB performance with crystalline FeOOH

Before FeOOH addition, the UASB reactors underwent a 5-day stabilization to achieve stable operation. The effluent COD values for RC, RB, and RA were 1430 mg/L, 1410 mg/L, and 1423 mg/L, respectively, indicating a similar degradation efficiency of approximately 93 % (Fig. 1a). After supplementing with FeOOH, reactor performance markedly improved, reducing COD to around 300 mg/L and doubling methane production from 1200 mL/d to 2500 mL/d (Fig. 1a-b). Performance enhancements varied depending on the crystalline forms of FeOOH, stabilizing after 20 days, and demonstrating significant differences in COD removal, as follows: RC (99.0 %, γ-FeOOH) > RB (98.3 %, β-FeOOH) > RA (97.1 %, α-FeOOH) (Fig. S1).

Anaerobic digestion was influenced by differences in crystalline structure, alongside other reactor parameters that ORP decreased and pH increased, correlating with enhanced digestion performance (Zhang et al., 2020). Each crystalline form of FeOOH could lower ORP from −11 mV to −50 mV and raise pH from 7.2 to 8.0 (Fig. 1c), indicating a more favorable reactor environment despite varying initial flow potentials (Fig. S2 and Table S1). The release of Fe ions from FeOOH was <10 mg/L (Fig. 1d), which suggests that the supplemented FeOOH remained relatively stable during operation (Qian et al., 2023; Weng et al., 2023). The order of Fe concentrations in the UASB reactors was RB (β-FeOOH) > RC (γ-FeOOH) > RA (α-FeOOH). Because the COD removal efficiency exceeding 97 %, ethanol and acetic acid concentrations remained low (Fig. 1e), with minimal variation in intermediate utilization efficiency across the different crystalline forms of FeOOH. DOM was further analyzed to uncover the influence of FeOOH crystals on molecular transformation. FeOOH altered the DOM composition, reducing the content of CHO compounds from 38.7 % to about 25 % (Figs. 1f and S3). In other words, FeOOH enhanced treatment efficiency across all categories of DOM, including aliphatic compounds, highly unsaturated compounds, polyphenols, and polycyclic aromatics. Notably, the proportion of aliphatic compounds decreased from 28 % to about 18 % (Figs. S4-S5 and Table S2-S4). Among the crystalline forms, RC with γ-FeOOH addition showed a lower molecular intensity in the effluent, correlating with its superior COD reduction performance (Fig. 1g).

2.2. Changes in granular sludge properties

To investigate further the influence of these crystalline forms of FeOOH on the properties of granular sludge, we evaluated coenzyme F_{420} content and ETS-INT activity in anaerobic digestion. An obvious enhanced coenzyme F_{420} content from 9.10 μmol/g MLSS (mixed liquor suspended solids) to approximately 15.0 μmol/g MLSS was observed with α-FeOOH and β-FeOOH addition. By comparison, the introduction of γ-FeOOH resulted in a remarkable 34.4 μmol/g MLSS, achieving the highest F_{420} level (Fig. 2a). The ETS-INT activity soared to about 75 μg/min/g MLSS following FeOOH addition but decreased over time. Once the reactors reached stable operation, the ETS-INT activity ranked as RB (β-FeOOH) > RC (γ-FeOOH) > RA (α-FeOOH). This pattern is consistent with the Fe content in EPS (Fig. 2b) and is influenced by the iron release from different crystalline forms (Fig. 1d). β-FeOOH released the highest levels of Fe, with 236.60 mg found in the effluent and 2163.46 mg accumulated in EPS. In contrast, α- and γ-FeOOH released lower amounts of Fe into both the effluent and EPS (Fig. S6 and Table S5). Despite this, the majority of Fe from β-FeOOH remained within the FeOOH phase throughout the operation.

FeOOH initially stimulated but later inhibited the EPS production, including protein and polysaccharide, as well as TOC, TC, and TN, which displayed a similar trend (Fig. 2b). Both α-FeOOH and β-FeOOH reduced the ratio of PN/PS (protein-to-polysaccharide), but it remained relatively stable in the presence of γ-FeOOH, indicating the minimal disruption to EPS. The EEM spectra of sludge EPS identified four components: aromatic protein substances (Peak A, Ex/Em = 270–290 nm/350–365 nm), fulvic acid substances (Peak B, Ex/Em = 240–243 nm/430–460 nm), humic acid substances (Peak C, Ex/Em = 320–350 nm/410–430 nm), and large molecular size hydrophobic compounds (Peak D, Ex/Em = 400–420 nm/470–480 nm) (Fig. 2c and Table S6) (He & Hur, 2015). Samples with added α-FeOOH and β-FeOOH experienced noticeable changes, while the intensity of the γ-FeOOH-amended sample remained relatively stable. Furthermore, α-FeOOH and β-FeOOH accumulated more large molecular size hydrophobic compounds compared to γ-FeOOH. This result suggests that α-FeOOH and β-FeOOH have a greater impact on EPS components than γ-FeOOH. FTIR analysis revealed new peaks for Fe-O-H (894 and 794 cm^{-1}) and Fe-O (631 cm^{-1}), indicating interactions between FeOOH and EPS following FeOOH addition (Figs. 2d and S7). Additionally, over time, the FTIR spectra of EPS became simpler, with the O-H and protein NH group peaks smoothing (2920–2850 cm^{-1}) and peak intensities diminishing, suggesting the formation of EPS-Fe complexes (Sun et al., 2009). However, due to the low Fe content in EPS (1.0 mg/g EPS), XPS and XRD analyses could not definitively identify the EPS-Fe complexes within EPS (Figs. S8-S9).

Crystalline FeOOH affects EPS through both Fe ion release and direct contact, as evidenced by Fe concentrations in the effluent and the Fe mass balance (Fig. S6 and Table S5). This is further supported by the uniform distribution of Fe throughout the granular sludge, as observed via SEM/EDS (Fig. 3), indicating that Fe ions penetrate and integrate with EPS. However, these FeOOH demonstrated minimal impact on the overall structure of the granular sludge. Despite the addition of FeOOH, the organic functional groups remained largely unchanged, as indicated by FTIR and XPS spectra similar to those of the initial sludge (Figs. 2e, S7, S10–S13 and Table S7). Additionally, the FeOOH properties closely resembled those at the initial addition (Figs. S14, S15), suggesting that both FeOOH and granular sludge maintained stability throughout the reactor operation.

2.3. Metagenomic insights into differentiated impact of FeOOH crystals

Given the varying iron release capabilities and surface characteristics of different FeOOH crystals, it was hypothesized that the microbial community structure would differ among these UASB reactors. Metagenomic analysis showed that alpha diversity indices - richness (Chao), diversity (Shannon), and evenness (Shannon even) - decreased in the order of R0 (control), RC (γ-FeOOH), RB (β-FeOOH), and RA (α-FeOOH) (Fig. 4a). These results indicate that, similar to the effects observed during reactor operation and sludge activity, FeOOH lowered microbial diversity. Among the crystals, γ-FeOOH had the least negative effect, resulting in a more stable and resilient microbial community. However, the alpha diversity indices were found not fully capture to the changes in the microbial community, which was remarkably altered by the presence of crystalline FeOOH. Although there were 8586 species common to all UASB reactors, the addition of FeOOH led to a significant reduction of 2636 unique species (Fig. 4b). Each type of FeOOH introduced distinct species, suggesting that the different crystals fostered a unique microbial community. Despite the reactor with γ-FeOOH showing similar alpha diversity indices to the control reactor without FeOOH, their species abundance differed the most (Fig. 4d).

The addition of FeOOH influenced the microbial community of granular sludge as follows: Euryarchaeota and Chloroflexi doubled in abundance. Methanogenic archaea from the Euryarchaeota phylum

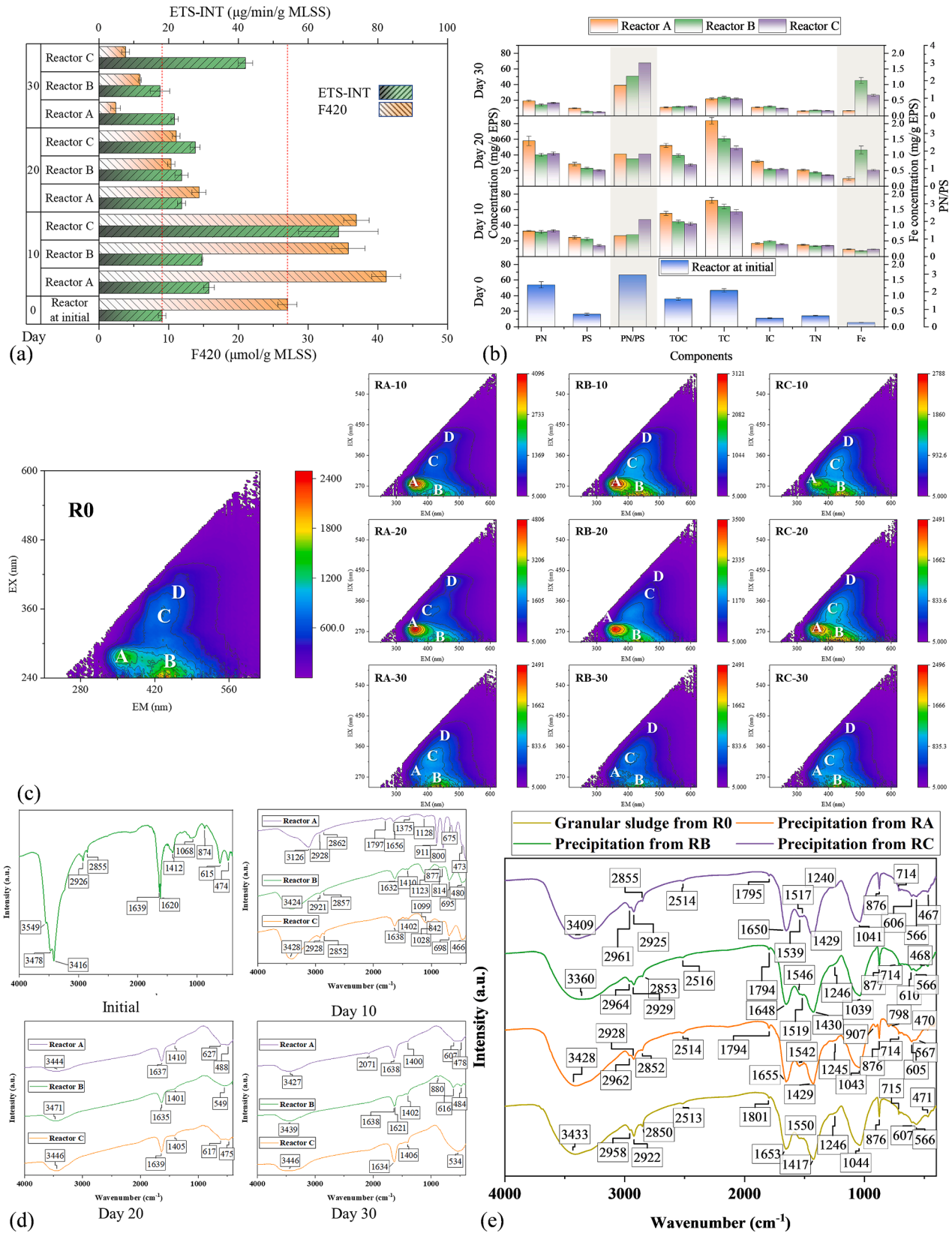

Fig. 2. Activity of the granular sludge. (a) F_{420} and ETS-INT activity. (b) Changes in EPS component concentration. (c) EEM spectra of the granular sludge EPS influenced by FeOOH. Four main peaks were marked as aromatic protein substances (Peak A, Ex/Em = 270–290 nm/350–365 nm), fulvic acid substances (Peak B, Ex/Em = 240–243 nm/430–460 nm), humic acid substances (Peak C, Ex/Em = 320–350 nm/410–430 nm), and large molecular size hydrophobic compounds (Peak D, Ex/Em = 400–420 nm/470–480 nm). (d) FTIR spectra of the granular sludge EPS influenced by FeOOH. (e) FTIR spectra of precipitates in reactors on Day 30.

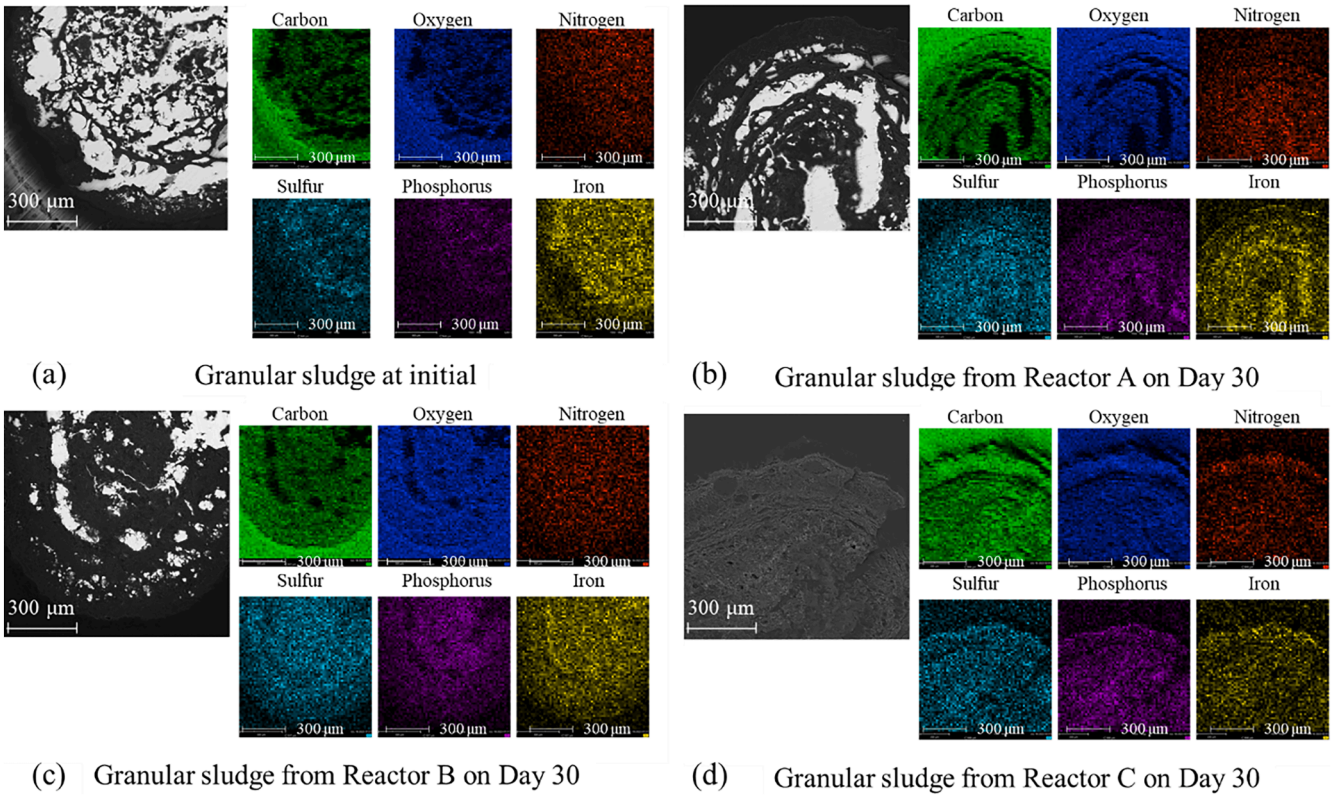

Fig. 3. SEM-EDS photographs of the sliced granular sludge in reactors (a) before FeOOH addition at initial and with (b) α-FeOOH, (c) β-FeOOH, and (d) γ-FeOOH addition on Day 30.

experienced an increase, reflecting the promoted coenzyme F_{420} content (Fig. S16). Similarly, the abundance of Chloroflexi and Cloacimonetes, known for degrading complex organic substances, also showed an increase. Conversely, the relative populations of Firmicutes and Planctomycetota decreased (Fig. 4c). Following the addition of FeOOH, there was an upregulation of ubiquinone-related proteins and the ABC-type Fe^{3+}-hydroxamate transport system (COG 0614), which are essential for Fe uptake, suggesting a metabolic pathway shift towards acquiring Fe(III) (Fig. 5a, b) (Al Shaer et al., 2020). However, a decline in microbial membrane-related metabolic activities was observed, suggesting a potential damage to the sludge in the presence of FeOOH. Despite the increased abundance of Euryarchaeota, known for its role in the transporter classification database (TCDB), the overall ETS activity decreased, primarily due to reduced contributions from Firmicutes and Planctomycetota (Figs. 5 and S17).

Crystalline forms of FeOOH expressed varying effects on microbial community development. In RC supplemented with γ-FeOOH, there was an enhancement in the species with methanogenic capability. Although *Methanothrix* levels decreased compared to those in reactors supplemented with β-FeOOH (RB) and α-FeOOH (RA), the abundance of *Mesotoga* increased, following the order RC (2.88 ‰) > RB (1.76 ‰) > RA (1.30 ‰). *Mesotoga* can reduce Fe(III) for methane production and is resilient to various stressors, highlighting its crucial role in maintaining methanogenic activity for waste treatment (Fig. S16) (De Vrieze et al., 2012; Shang et al., 2020). Additionally, the addition of γ-FeOOH induced an increase in the abundances of *Mesotoga, Syntrophus,* and *Chloroflexi*, which are known to facilitate DIET for improved complex organic matter degradation and methane production (Giangeri et al., 2023). This enhancement in DIET was further supported by the presence of components related to DIET, such as cytochrome-associated proteins and P450 enzymes (Zhang et al., 2023). The unique rise in enzyme activities, such as gastricsin, gastrokine, H^+/K^+-exchanging ATPase, and glutathione S-transferase further enhanced the digestion performance of RC (Fig. S17). Moreover, the microbial community in RC demonstrated robust growth, excelling in glycan biosynthesis and metabolism, as well as lipid metabolism – crucial for its enhanced anaerobic digestion efficiency (Fig. S18), with lower molecules production in effluent and higher COD removal.

3. Discussion

Iron oxides can enhance anaerobic digestion by lowering the ORP, generating H_2, facilitating DIET, and optimizing the microbiome, all of which benefit the digestion process. Our findings indicate that the digestion performance of UASB reactors was influenced by the crystalline forms of FeOOH, with γ-FeOOH proving to be particularly effective. This observation is consistent with previous studies, further highlighting the importance of crystalline structure (Hao et al., 2017; Zhao et al., 2018). In this study, each form of FeOOH exhibited distinct crystalline surfaces: α-FeOOH featured (110), (130), and (111) surfaces; β-FeOOH had (110), (220), and (310) surfaces; and γ-FeOOH was characterized by (031), (120), and (080) surfaces (Figs. S7, S19 and S20). The similarities in the crystalline surfaces of α-FeOOH and β-FeOOH resulted in comparable effects on anaerobic digestion, despite their different flow potentials, whereas the unique crystalline surfaces of γ-FeOOH led to distinct behaviors.

The crystalline structures impacted reactor operation through both indirect interactions, such as Fe ion release, and direct interactions between sludge granules and FeOOH, all rooted in the crystalline properties. These interactions altered EPS components, DIET processes, and microbial metabolisms, manifesting as biocompatibility and biotoxicity, ultimately influencing digestion performance. The release of Fe ions from FeOOH varied over the course of the operation (Fig. 1d). The release followed the sequence α-FeOOH > γ-FeOOH > β-FeOOH, aligning with the stability grades of crystalline FeOOH (Poulton & Canfield, 2005; Liu et al., 2023a). The order of Fe ion release partially

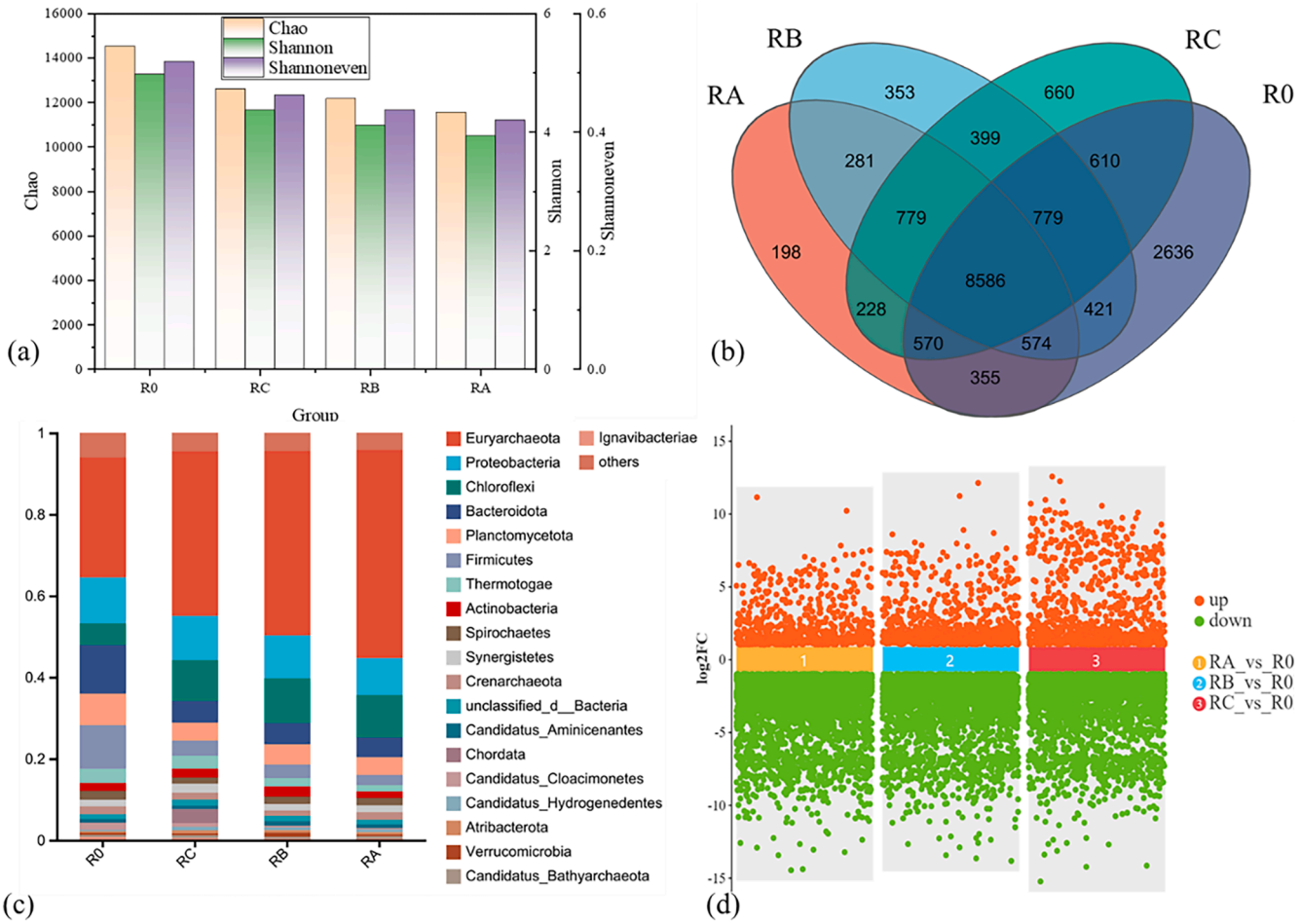

Fig. 4. Effects of FeOOH on the microbial community. (a) Alpha diversity index. (b) Venn diagram of species differences with FeOOH addition. (c) Barplot of microbial community abundance. (d) Scatter plot comparing species abundance differences with the control group.

explains the accumulation of Fe in EPS, as ion release is a key indirect transport mechanism. Additionally, differences in direct contact influence EPS properties, which is evident from the unpaired Fe in the effluent and Fe accumulation in EPS. This finding underscores the impact of crystalline FeOOH structure on EPS characteristics. Although the final Fe loading was lower compared to previous studies (Abdelsalam & Samer, 2019; Dehhaghi et al., 2019; Huangfu et al., 2019), remarkable changes in EPS function and microbiome were observed.

Among the forms studied, γ-FeOOH demonstrated the highest electrocatalytic activity due to its optimal reactivity band gaps (Seabold & Choi, 2012). This characteristic could enhance DIET processes, as shown by the increased levels of proteins such as ubiquitin, cytochrome c, and P450 families. Additionally, γ-FeOOH's OH terminations and lower surface energy reduced contact damage compared to α-FeOOH and β-FeOOH, which have OH/Fe terminations (Otte et al., 2012). These properties granted γ-FeOOH superior biocompatibility, leading to a more stable and efficient community structure. This environment supported the growth of methane-producing and DIET-supporting microbes and enriched unique biosynthesis and metabolism (Fig. S17). Although FeOOH is inherently less toxic to anaerobic digestion than other iron (hydro)oxides (Lefevre et al., 2016), γ-FeOOH stands out for its exceptional biocompatibility, resulting in the best digestion performance. This feature is crucial in enhancing the overall efficiency of the microbial processes within the reactor.

Iron oxides play a crucial role in enhancing anaerobic digestion, yet the variations in their crystalline structures, which determine their properties, are often overlooked. This study focused on the specific effects of FeOOH, the predominant component on the surface of iron oxides, which forms various crystalline structures upon exposure to water. With its consistent Fe(III) valence composition and diverse crystalline forms, FeOOH offers stability and a high valence state that differentiate it from other iron oxides. Using FeOOH mitigates common issues like hydrogen production and reactions with influent, allowing for an examination of how its crystalline structures influence digestion performance.

4. Conclusions

This study highlights the intricate relationship between the crystalline structure of FeOOH and its impact on anaerobic digestion. Each form of FeOOH, characterized by distinct properties, uniquely influences the treatment process through mechanisms such as Fe ion release and surface interactions. Even subtle variations in crystal structure can significantly affect EPS functions, DIET processes, and microbial metabolisms, thereby impacting the overall efficiency of anaerobic digestion. This study demonstrates that while iron oxides prove effective in anaerobic digestion, attention must be paid to its crystalline form and biocompatibility. By addressing the knowledge gap regarding crystalline structures and their applications, engineers are now equipped to make more informed decisions to enhance anaerobic digestion processes.

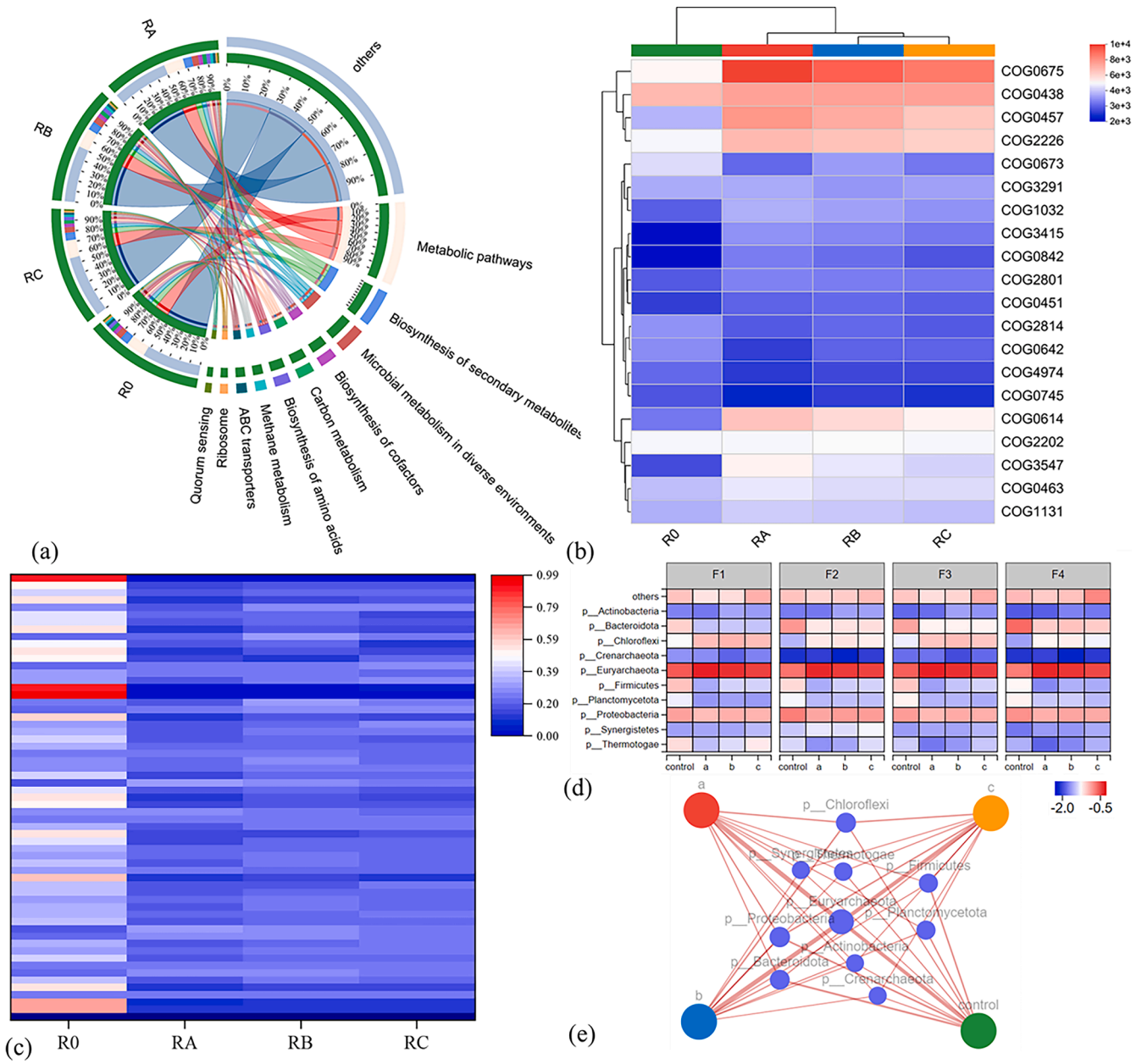

Fig. 5. Effects of FeOOH on microbial functions. (a) Distribution of KEGG functions in relation to FeOOH. (b) COG difference heatmap. (c) Membrane-related KEGG heatmap. (d) Contributions of key species to TCDB functions in each group classified as F1: Primary active transporters, F2: Electrochemical potential-driven transporters, F3: Incompletely characterized transport systems, F4: Channels and pores. (e) Network diagram showcasing interspecies interactions within microbial communities.

5. Materials and methods

5.1. Reactor startup and operation

UASB reactors with a working volume of 7.2 L (100 cm height and 10 cm diameter), and equipped with a three-phase separator (Fig. S21), were utilized in this study. These reactors had been in operation for over a year before the experiment. The influent, sourced from a reconstituted tobacco leaf production waste, had an initial chemical oxygen demand (COD) of 150,000 mg/L, which was diluted to 15,000 mg/L and adjusted to a pH of approximately 7.0 using $NaHCO_3$ (Table S8). The influent and recirculation flows were maintained at 1.76 mL/min and 15.06 mL/min, respectively, achieving an up-flow velocity of 0.3 m/h and a volumetric loading rate of 5.26 kg COD/m^3/d. A water jacket was used to maintain the UASB reactors at a temperature of 25 ± 2 °C. Over a 30-day period, the reactors were classified as R0 (before FeOOH addition), RA (with α-FeOOH addition), RB (with β-FeOOH addition), and RC (with γ-FeOOH addition). Before inoculation into the reactors, the granular sludge was initially mixed for consistency, and then underwent a 5-day stabilization phase. Each reactor contained 2 L of granular sludge at a bed height of 35 cm. FeOOH was introduced at a concentration of 5 g/L Fe equivalent.

5.2. Granular sludge characterization

To evaluate the activity of granular sludge, fluorescence measurements for coenzyme F_{420} and electron transfer system (ETS) activity were conducted at given time intervals (Ma et al., 2013). At the end of the experiment, scanning electron microscopy coupled with energy dispersive X-ray spectroscopy (SEM-EDS, Phenom ProX, the

Netherlands) was used to analyze the morphology and elemental composition of the granular sludge and precipitates.

5.3. EPS extraction and analysis

EPS were extracted using a heating method as follows: 1) 10 g of granular sludge was centrifuged in a 50 mL tube at 8000 × *g* for 5 min, washed three times with a 0.9 % NaCl solution, and then dehydrated. 2) The sludge particles were resuspended in 30 mL of 0.9 % NaCl solution and heat-treated at 80 °C for 1 h, followed by centrifugation at 8000 × *g* for 15 min. 3) The supernatant obtained was filtered through a 0.22 μm filter to remove any microbes, and the resulting total EPS was freeze-dried and stored at −20 °C (Zhu et al., 2012). Detailed procedures regarding the EPS analysis are available in the Supplementary Materials.

5.4. DNA extraction, fragmentation, and annotation

A metagenomic analysis using whole-genome sequencing was performed on the granular sludge to elucidate the development of microbial community at Shanghai Biopharm Co., China. The quality and integrity of the extracted DNA were assessed via 1 % agarose gel electrophoresis. The DNA was then fragmented to approximately 350 base pairs using the Covaris M220 instrument, which is critical for efficient sequencing preparation. The resulting sequencing data were annotated for species and functional classification using several comprehensive databases, including the non-redundant protein database (NR), clusters of orthologous groups of proteins (COG), and the Kyoto Encyclopedia of Genes and Genomes (KEGG).

5.5. Chemical analysis

COD was measured following the standard potassium dichromate (COD_{Cr}) method (Chinese national standard HJ 828–2017). The volume of gaseous product was assessed through water displacement, while its composition was analyzed using a portable infrared detector. pH and ORP were measured with a standard pH meter. Iron ion concentrations were determined using an inductively coupled plasma optical emission spectrometer (ICP-OES, Opmita 7300 DV, PerkinElmer Corp., U.S.). VFA and ethanol content was analyzed by gas chromatography, employing a DB-FFAP column and a flame ionization detector (FID) detector, with nitrogen as the carrier gas. DOM was extracted using solid-phase extraction (SPE) for desalination and enrichment, then analyzed with high-resolution mass spectrometry (HRMS) on an Orbitrap mass spectrometer. Electrospray ionization (ESI) in negative mode covered a range of 150 to 1200 *m/z*. Molecular formulae were represented using Van Krevelen diagrams, based on O/C and H/C ratios.

CRediT authorship contribution statement

Han-Quan Wen: Writing – original draft, Investigation, Funding acquisition, Formal analysis, Data curation. **Guan-Lin Chen:** Investigation, Formal analysis, Data curation. **Yu-Sheng Li:** Writing – review & editing, Validation, Conceptualization. **Tian Tian:** Writing – review & editing, Supervision. **Yuan Pan:** Writing – review & editing, Validation. **Han-Qing Yu:** Writing – review & editing, Supervision, Funding acquisition, Conceptualization.

Declaration of competing interest

The authors declare that they have no known competing financial interests or personal relationships that could have appeared to influence the work reported in this paper.

Acknowledgments

The authors would like to thank the National Natural Science Foundation of China (52200075, 51821006, 52192684, 52170057), the China Postdoctoral Science Foundation Funded Project (2022M713041) and National Key R&D Plan of China (2023YFC3207602) for supporting this work.

Supplementary materials

Supplementary material associated with this article can be found, in the online version, at doi:10.1016/j.wroa.2024.100286.

Data availability

Data will be made available on request.

References

Abdelsalam, E.M., Samer, M., 2019. Biostimulation of anaerobic digestion using nanomaterials for increasing biogas production. Rev. Environ. Sci. Biotechnol. 18 (3), 525–541.
Alatalo, S.M., Daneshvar, E., Kinnunen, N., Meščeriakovas, A., Thangaraj, S.K., Jänis, J., Tsang, D.C.W., Bhatnagar, A., Lähde, A., 2019. Mechanistic insight into efficient removal of tetracycline from water by Fe/graphene. Chem. Eng. J. 373, 821–830.
Ali, F.M., Hmadeh, M., O'Brien, P.G., Perovic, D.D., Ozin, G.A., 2016. Photocatalytic properties of all four polymorphs of nanostructured iron oxyhydroxides. ChemNanoMat 2 (11), 1047–1054.
Al Shaer, D., Al Musaimi, O., de la Torre, B.G., Albericio, F., 2020. Hydroxamate siderophores: natural occurrence, chemical synthesis, iron binding affinity and use as Trojan horses against pathogens. Eur. J. Med. Chem. 208, 112791.
Bird, L.J., Bonnefoy, V., Newman, D.K., 2011. Bioenergetic challenges of microbial iron metabolisms. Trends Microbiol. 19 (7), 330–340.
Brown, G.E., Henrich, V.E., Casey, W.H., Clark, D.L., Eggleston, C., Felmy, A., Goodman, D.W., Grätzel, M., Maciel, G., McCarthy, M.I., Nealson, K.H., Sverjensky, D.A., Toney, M.F., Zachara, J.M., 1999. Metal oxide surfaces and their interactions with aqueous solutions and microbial organisms. Chem. Rev. 99 (1), 77–174.
Cheng, J., Zhu, C., Zhu, J., Jing, X., Kong, F., Zhang, C., 2020. Effects of waste rusted iron shavings on enhancing anaerobic digestion of food wastes and municipal sludge. J. Clean Prod. 242, 118195.
De Vrieze, J., Hennebel, T., Boon, N., Verstraete, W., 2012. Methanosarcina: the rediscovered methanogen for heavy duty biomethanation. Bioresour. Technol. 112, 1–9.
Dehhaghi, M., Tabatabaei, M., Aghbashlo, M., Kazemi Shariat Panahi, H., Nizami, A.-S., 2019. A state-of-the-art review on the application of nanomaterials for enhancing biogas production. J. Environ. Manag. 251, 109597.
Dong, Y., Sanford, R.A., Chang, Y.J., McInerney, M.J., Fouke, B.W., 2017. Hematite reduction buffers acid generation and enhances nutrient uptake by a fermentative iron reducing bacterium, *Orenia metallireducens* strain Z6. Environ. Sci. Technol. 51 (1), 232–242.
Furcas, F.E., Lothenbach, B., Mundra, S., Borca, C.N., Albert, C.C., Isgor, O.B., Huthwelker, T., Angst, U.M., 2023. Transformation of 2-line ferrihydrite to goethite at alkaline pH. Environ. Sci. Technol. 57 (42), 16097–16108.
Giangeri, G., Tsapekos, P., Gaspari, M., Ghofrani-Isfahani, P., Hong Lin, M.K.T., Treu, L., Kougias, P., Campanaro, S., Angelidaki, I., 2023. Magnetite alters the metabolic interaction between methanogens and sulfate-reducing bacteria. Environ. Sci. Technol. 57 (43), 16399–16413.
Hao, X., Wei, J., van Loosdrecht, M.C.M., Cao, D., 2017. Analysing the mechanisms of sludge digestion enhanced by iron. Water Res. 117, 58–67.
He, W., Hur, J., 2015. Conservative behavior of fluorescence EEM-PARAFAC components in resin fractionation processes and its applicability for characterizing dissolved organic matter. Water Res. 83, 217–226.
Huangfu, X., Xu, Y., Liu, C., He, Q., Ma, J., Ma, C., Huang, R., 2019. A review on the interactions between engineered nanoparticles with extracellular and intracellular polymeric substances from wastewater treatment aggregates. Chemosphere 219, 766–783.
Kato, S., Hashimoto, K., Watanabe, K., 2012. Microbial interspecies electron transfer via electric currents through conductive minerals. Proc. Natl. Acad. Sci. 109 (25), 10042–10046.
Kleber, M., Bourg, I.C., Coward, E.K., Hansel, C.M., Myneni, S.C.B., Nunan, N., 2021. Dynamic interactions at the mineral–organic matter interface. Nat. Rev. Earth Environ. 2 (6), 402–421.
Lefevre, E., Bossa, N., Wiesner, M.R., Gunsch, C.K., 2016. A review of the environmental implications of *in situ* remediation by nanoscale zero valent iron (nZVI): behavior, transport and impacts on microbial communities. Sci. Total Environ. 565, 889–901.
Liu, L., Sassi, M., Zhang, X., Nakouzi, E., Kovarik, L., Xue, S., Jin, B., Rosso, K.M., De Yoreo, J.J., 2023a. Understanding the mechanisms of anisotropic dissolution in metal oxides by applying radiolysis simulations to liquid-phase TEM. Proc. Natl. Acad. Sci. 120 (23), e2101243120.
Liu, Y., Ding, Y., Sheng, A., Li, X., Chen, J., Arai, Y., Liu, J., 2023b. Fe(II)-catalyzed transformation of ferrihydrite with different degrees of crystallinity. Environ. Sci. Technol. 57 (17), 6934–6943.

Ma, J., Quan, X., Si, X., Wu, Y., 2013. Responses of anaerobic granule and flocculent sludge to ceria nanoparticles and toxic mechanisms. Bioresour. Technol. 149, 346–352.
Otte, K., Schmahl, W.W., Pentcheva, R., 2012. Density functional theory study of water adsorption on FeOOH surfaces. Surf. Sci. 606 (21), 1623–1632.
Poulton, S.W., Canfield, D.E., 2005. Development of a sequential extraction procedure for iron: implications for iron partitioning in continentally derived particulates. Chem. Geol. 214 (3), 209–221.
Qian, A., Lu, Y., Zhang, Y., Yu, C., Zhang, P., Liao, W., Yao, Y., Zheng, Y., Tong, M., Yuan, S., 2023. Mechanistic insight into electron transfer from Fe(II)-bearing clay minerals to Fe (hydr)oxides. Environ. Sci. Technol. 57 (21), 8015–8025.
Seabold, J.A., Choi, K.S., 2012. Efficient and stable photo-oxidation of water by a bismuth vanadate photoanode coupled with an iron oxyhydroxide oxygen evolution catalyst. J. Am. Chem. Soc. 134 (4), 2186–2192.
Shang, H., Daye, M., Sivan, O., Borlina, C.S., Tamura, N., Weiss, B.P., Bosak, T., 2020. Formation of zerovalent iron in iron-reducing cultures of *Methanosarcina barkeri*. Environ. Sci. Technol. 54 (12), 7354–7365.
Sun, X.F., Wang, S.G., Zhang, X.M., Paul Chen, J., Li, X.M., Gao, B.Y., Ma, Y., 2009. Spectroscopic study of Zn^{2+} and Co^{2+} binding to extracellular polymeric substances (EPS) from aerobic granules. J. Colloid Interface Sci. 335 (1), 11–17.
Taillefert, M., Beckler, J.S., Carey, E., Burns, J.L., Fennessey, C.M., DiChristina, T.J., 2007. *Shewanella putrefaciens* produces an Fe(III)-solubilizing organic ligand during anaerobic respiration on insoluble Fe(III) oxides. J. Inorg. Biochem. 101 (11), 1760–1767.
Tian, T., Yu, H.Q., 2020. Iron-assisted biological wastewater treatment: synergistic effect between iron and microbes. Biotechnol. Adv. 44, 107610.
Wang, D., Pan, Q., Yang, J., Gong, S., Liu, X., Fu, Y., 2024. Effects of mixtures of engineered nanoparticles and cocontaminants on anaerobic digestion. Environ. Sci. Technol. 58 (6), 2598–2614.
Wang, M., Zhao, Z., Niu, J., Zhang, Y., 2019. Potential of crystalline and amorphous ferric oxides for biostimulation of anaerobic digestion. ACS Sustain. Chem. Eng. 7 (1), 697–708.
Weng, H., Yang, Y., Zhang, C., Cheng, M., Wang, W., Song, B., Luo, H., Qin, D., Huang, C., Qin, F., Li, K., 2023. Insight into FeOOH-mediated advanced oxidation processes for the treatment of organic polluted wastewater. Chem. Eng. J. 453, 139812.
Zhang, J., Qu, Y., Qi, Q., Zhang, P., Zhang, Y., Tong, Y.W., He, Y., 2020. The bio-chemical cycle of iron and the function induced by ZVI addition in anaerobic digestion: a review. Water Res. 186, 116405.
Zhang, X., Liu, Y., Zhou, Q., Bai, Y., Li, R., Li, T., Li, J., Alessi, D.S., Konhauser, K.O., 2023. Exogenous electroactive microbes regulate soil geochemical properties and microbial communities by enhancing the reduction and transformation of Fe(III) minerals. Environ. Sci. Technol. 57 (20), 7743–7752.
Zhao, Z., Li, Y., Quan, X., Zhang, Y., 2017. Towards engineering application: potential mechanism for enhancing anaerobic digestion of complex organic waste with different types of conductive materials. Water Res. 115, 266–277.
Zhao, Z., Zhang, Y., Li, Y., Quan, X., Zhao, Z., 2018. Comparing the mechanisms of ZVI and Fe_3O_4 for promoting waste-activated sludge digestion. Water Res. 144, 126–133.
Zhou, W., Zhou, J., Feng, X., Wen, B., Zhou, A., Liu, P., Sun, G., Zhou, Z., Liu, X., 2023. Antimony isotope fractionation revealed from exafs during adsorption on Fe (oxyhydr)oxides. Environ. Sci. Technol. 57 (25), 9353–9361.
Zhu, L., Qi, H.Y., Lv, M.L., Kong, Y., Yu, Y.W., Xu, X.Y., 2012. Component analysis of extracellular polymeric substances (EPS) during aerobic sludge granulation using FTIR and 3D-EEM technologies. Bioresour. Technol. 124, 455–459.